Improving Practical Performance of Single-tip-optical-fibre Probing for Measurement of Bubble-Swarm Motion and Properties in a Large Diameter Bubble Column

Yuki Mizushima[a], Takayuki Saito[*b]

[a] Graduate school of engineering, Shizuoka university Shizuoka University, 3-5-1 Johoku, Naka-ku, Hamamatsu, Shizuoka, Japan
[b] Graduate School of Science and Technology, Shizuoka University, 3-5-1 Johoku, Naka-ku, Hamamatsu, Shizuoka, Japan
ttsaito@ipc.shizuoka.ac.jp

Bubble column reactors are frequently applied to chemical plants and other industrial plants. To elucidate the practical properties of the bubble columns, the heat and mass transfer phenomena in consideration of the average bubble diameters and average void fractions have been investigated. Although the macroscopic flow structure and the fluctuation over a long time can be well-described, knowledge of microscopic and instantaneous flow structures is still insufficient experimentally and numerically. To solve this long-pending question, an optical fibre probe (OFP) is very useful practically. The OFP measures bubble diameters, velocities, and local void fractions simultaneously. Because of its intrusion, the OFP can successfully measure bubbles even in cases of high bubble density. Still, the OFP remains the measurements for laboratory conditions.

In this study, we originally analyse practical signals of a Single-Tip Optical fibre Probe (S-TOP) in a bubble column measurement. One of the authors already developed a numerical simulator, i.e. a ray tracing simulator. It rationally and quantitatively analyses optic signals delivered from the S-TOP. By using this, we can rapidly improve the S-TOP measurement. We discuss potential of this simulator through analysis of signals of bubble measurement in a large bubble column.

First, the S-TOP measurement in a bubble column (approximately 380 mm in diameter and 1500 mm in height) was conducted. Second, the analysis for obtained signals was conducted numerically and empirically. Finally, we discussed practical performance of OFP for the bubbly flow measurement based on the analytical results.

1. Introduction

Gas–liquid two-phase flows are frequently encountered in a wide range of industrial fields: e.g. a chemical reactor for phenol production, a hot metal cooling process, and waste water treatment. Investigating the bubble properties and motions is essential to improve and maintain their performances. For this purpose, optical fibre probing (OFP) is reliably applicable. Since the 1970s, researchers invented some types of the OFP, and reported their pleasant results of measurement for bubbly flows. It is concluded that bubbles with a size ranging from about 1 to 5 mm (equivalent sphere diameter) are appropriate for conventional OFP methods. However, most were conducted under laboratory conditions: a small bubble column, a low bubble concentration and mono-dispersed bubbles in quiescent liquid. Hence, the optical signals were clear and high quality. In the industrial use of OFPs, such conditions are rare (imagine: bubbles' motions in a large diameter bubble column), and the probe signals inevitably include many types of noise. Although a bubble detection process is essential in the optical probing, sometimes the signals corresponding to the bubble cannot be distinguished from noise, and the misdetection of the bubbles makes measurement accuracy decline. Previous studies corrected the inaccuracy by a statistical way; i.e. introducing a calibration factor. Limits of application of the statistical method to a large diameter bubble column (practical

bubble column) have to be recognized. In the present study, we overcome this issue. We computationally analysed signals delivered from a Single-Tip Optical fibre Probe (S-TOP) in a large diameter bubble column, and educed information latent in the noise. In fact, a pre-signal which sharply appeared just before the S-TOP touches a frontal surface of a bubble indicated the position pierced by the S-TOP. By using this, we can originally detect where the OFP has touched bubble in a bubbly flow. We clarified the properties of the pre-signal and spike-noise, which were avoided as major noises of OFP. Then we discussed practical performance of the S-TOP for the bubble column measurement.

2. Single-Tip Optical fibre Probe

2.1 Optics

The optical system used in the present S-TOP measurement is illustrated in Figure 1. A laser diode (a) (3 mW power, 635 nm wavelength) was used as the light source of the S-TOP. The laser beams passed through a beam splitter (b) and were focused on the light-source-side end of the S-TOP by an objective lens (c). The focused laser beams entered the optical fibre and reached the S-TOP sensing tip (d). The laser beams reaching the tip surface were returned/emitted to/from the tip positioned in water/air, due to the Snell's law. Some of the returned beams entered a photomultiplier (f) through a polarizer (e) eliminating unwanted beams (the beams directly scattered from the lens or beam splitter). Thus, we obtained the electrical signal output from the photomultiplier. In succession, we analyse the ON/OFF signals and simultaneously obtained the velocities, diameters and number densities of the bubbles.
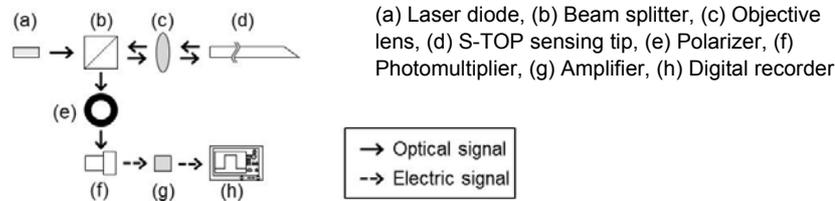

(a) Laser diode, (b) Beam splitter, (c) Objective lens, (d) S-TOP sensing tip, (e) Polarizer, (f) Photomultiplier, (g) Amplifier, (h) Digital recorder

Figure 1: Optical system of the S-TOP measurement.

The schematic and a micrograph of the S-TOP used in this study are shown in Figures. 2. The S-TOP was made from a plain optical fibre (synthetic quartz fibre of the step index type with a core diameter of 190 µm and a clad thickness of 5 µm). The sensing tip was smoothly ground into a wedge with an angle of 35°. The S-TOP was fixed in a stainless steel capillary (inner diameter: 230 µm, outer diameter: 450 µm), and the S-TOP and capillary were installed in a reinforcement tube of stainless steel (inner diameter: 1 mm, outer diameter: 3 mm).

(a) Schematic of the probe

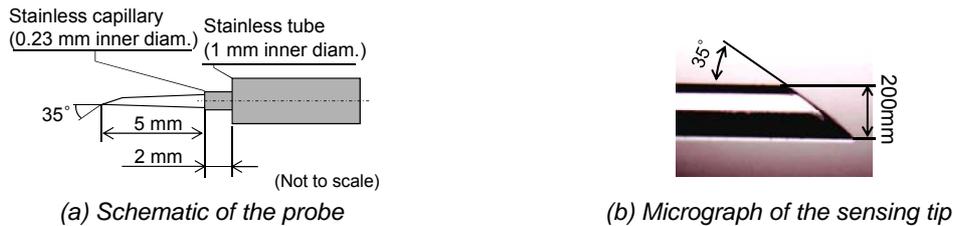*(b) Micrograph of the sensing tip*

Figure 2. Structure of the S-TOP.

2.2 Signal processing

A typical signal obtained in the bubble measurement via the S-TOP is shown in Figure. 3. Before the wedge-shaped tip penetrates a bubble, the output voltage indicated a liquid-phase output level, at time of (1) as marked with arrow (1). Being covered gradually with the gas phase, the wedge-shaped tip was completely positioned in the bubble; the output voltage took a gas-phase output level, at time of (2) as marked with arrow (2). After the S-TOP finished dwelling in the bubble, the output voltage returned to the baseline value again, at time of (3) as marked with arrow (3). Here, the gradient of the steep surge in Figure 3 was proportional to the vertical velocity component of the interface; the velocity was calculated from the following equation,

$$U = \alpha \times g_{rd} \text{,}$$

(1)

where g_{rd} (V/s) is the gradient of an upslope of the signal, and α (m/V) is a proportionality coefficient between U (m/s) and g_{rd} (V/s). We obtain U as a bubble velocity on the assumption that the interface velocity stays at a constant value during piercing. The signal also provides the time of starting to penetrate the bubble and the time of finishing dwelling; therefore pierced chord length is calculated by Eq. (2),

$$L = U \times \left(t_e - t_s \right)$$

(2)

where L (mm) is the pierced chord length, t_s (s) is the time of starting to penetrate the bubble, and t_e (s) is the time of ending to penetrate the bubble.
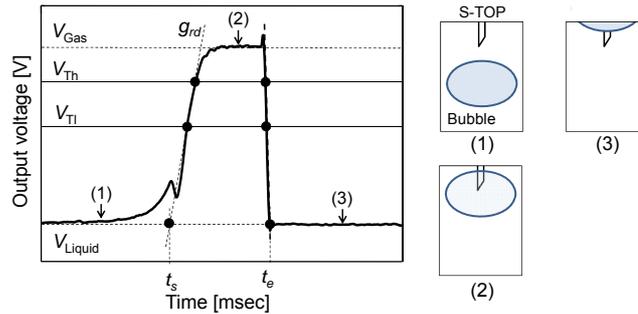

Figure 3. Typical output signal of the S-TOP in the bubble measurement.

3. 3D ray tracing simulator

Our 3D ray tracing simulator rationally and quantitatively analyses optic signals delivered from the S-TOP in consideration of not only every ray trajectory but also energy of every ray. Figure 4 outlines the 3D ray tracing simulator. In this simulator, the light waves were transposed to ray segments. We developed a new algorithm to achieve both numerical accuracy and reduction of computational time. For modelling, the S-TOP optics was rendered by not polygons but smoothly numerical models of four surfaces: the inlet surface, lateral faces (fibre-clad and core), and outlet surface. Each object linked to the neighbour objects. If we simply use many meshes without the links, it has to calculate all surfaces at the searching step of the next cross point of a ray and a surface. By this linked model, our simulator considerably reduced the computational time. Three-dimensional reflection and refraction of the rays were numerically computed under the Snell's law. Energy of every ray was defined by Fresnel's equation as a function of the incident/reflection angles, polarizations, and the transmissivity/reflectivity on the interfaces among the fibre core, air, and water. According to circumstances, the specific amounts of the rays returned from the S-TOP tip; i.e. the returned beams. We defined this value as an S-TOP signal of this simulation.

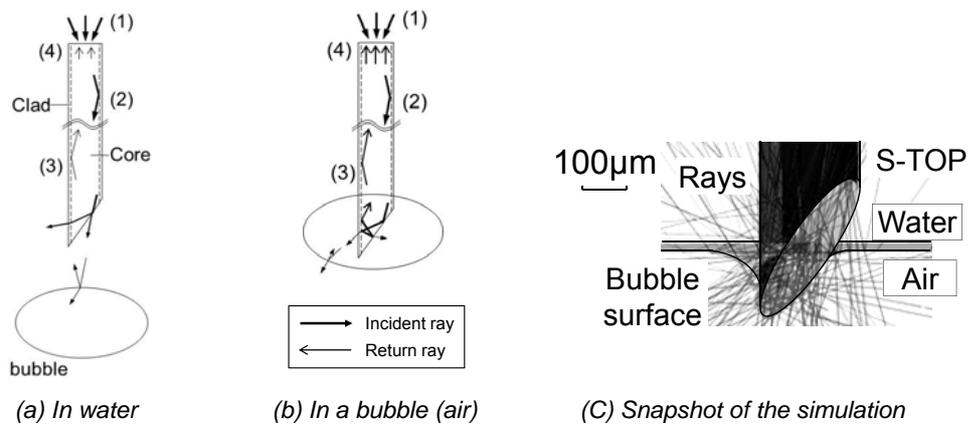(a) In water   (b) In a bubble (air)   (C) Snapshot of the simulation

Figure 4. Schematic of the numerical simulation. (1) The rays are introduced. (2) The rays iterate total reflection. (3) Depending on the conditions, rays return. (4) The returned rays' energy is sum up.

4. Experimental apparatus

4.1 Large diameter bubble column measurement

A schematic diagram of the experimental setup employed in the bubble column experiments is shown in Figure 5. An acrylic bubble column of 380 mm in inner diameter and 1500 mm in height was covered with an acrylic water jacket of 440 mm × 440 mm in square cross section and 1605 mm in height. The bubble column was equipped with a perforated plate (diameter of pores: 1.0 mm; equilateral triangular pitch: 10 mm; the number of pores: 1240). Tap water was supplied from a water reservoir into the bubble column through the water inlet. Compressed air, supplied from a compressor, was controlled with a mass flow controller (mass flow rate 37 NL/min) and injected into an air chamber (380 mm in diameter and 200 mm in height). The air chamber was equipped with a resistance material (multi-layered fibres) in order to minimize the fluctuation of the gas pressure and to uniform the gas flow distribution.

(1) S-TOP, (2) Water inlet, (3) Water jacket,(4) Perforated plate, (5) Water reservoir, (6) Compressor, (7) Mass flow meter, (8) Air chamber, (9) Laser diode, (10) Beam splitter, (11) Photo multiplier, (12) A/D converter, (13) PC

Figure 5. Setup for the bubble column measurement (the image is captured by SONY digital handy-cam).

4.2 Single bubble measurement

The experimental setup employed in this study is illustrated in Figure 6. A single bubble was launched from a hypodermic needle (0.19 mm inner diameter) (g) into a vessel (f) of 150 × 150 × 300 mm^3, filled with ion-exchanged and degassed tap water. The bubble ascended vertically and touches the S-TOP (a) fixed above the needle. The optical signals were stored by the recorder (i). The bubble measurement process was captured with two high-speed video cameras (d) (e). These devices were synchronized by function generator (h).

(a) S-TOP, (b) Halogen light source 1, (c) Halogen light source 2, (d) High-speed video camera 1, (e) High-speed video camera 2, (f) Acrylic water vessel, (g) Needle, (h) Function generator, (i) Recorder, (j) Optical system, (k) Flow meter, (l) Cylinder
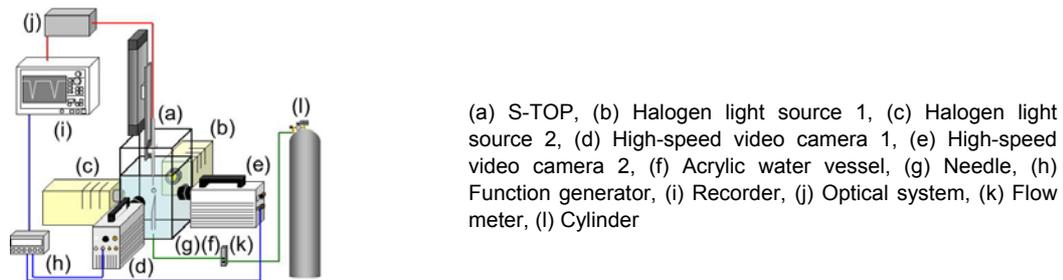
Figure 6. Experimental setup for the single bubble measurement.

5. Results and discussions

5.1 Inevitable noisy-signals in the S-TOP measurement of "real" bubbly flow.

In industrial use of the S-TOP, the signals include many types of noise. They are grouped into two major categories: electric noise and optical noise. The former one is owing to the transient responses of electrical units and the power supply. They are easily separated with electronic filtering. The latter is caused by mechanical oscillations of the optical units and disturbance from backgrounds (fluorescent lights, sunlight, etc.) into the photomultiplier. Most effects of them are prevented by isolation of the measurement systems. Figure 7 shows typical signals delivered from the S-TOP (at 600 mm in height) in the bubble column measurement, after removing above noises. However, the S-TOP signals are still noisy.
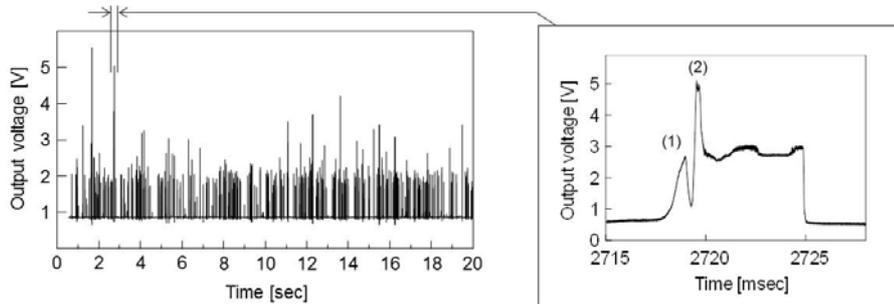
Figure 7. Time series output signal from the S-TOP in the bubbly flow. A typical burst signal is extracted.

5.2 Computational analysis of the S-TOP signal via ray tracing simulation.

Figure 8 (a) shows typical snapshots and signal patterns obtained from the single bubble measurement. Similar to the signal in Figure 7, two characteristic peaks ((1) and (2) in the figure) were detected.

To describe when, where, and how the peaks arose, we simulated the same condition as the experiment via ray tracing simulation (Figure 8(b)). The modelled bubble was moved in steps of 10 µm. 10,000 initial incident rays and the numerous derived rays by every reflection were computed per each step. The bubble deformation obtained from the visualized images in the experiment was considered in the simulator.

(a) Result from the experiment
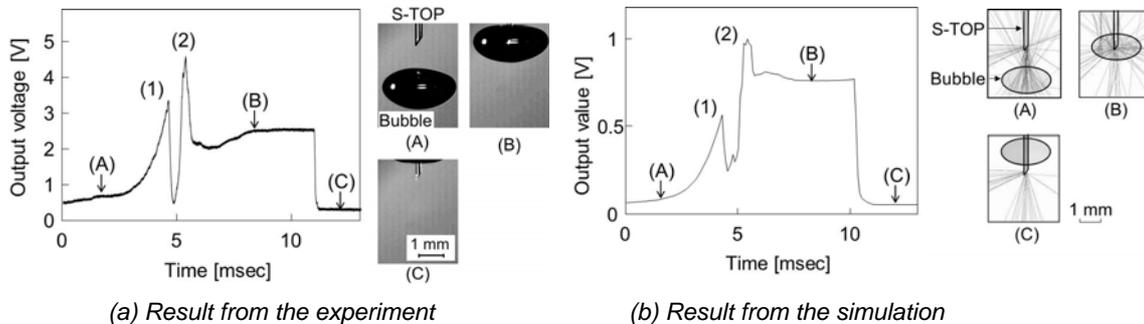
(b) Result from the simulation

Figure 8. Typical experimental result and numerical result of the S-TOP.

We investigated the wave patterns carefully and found that the noise (marked as (1), (2) in Figures 7 and 8) arise from optical phenomena of the S-TOP and air-water interface. The mechanisms are as follows:
(1) Pre-signal
A pre-signal appears just before the S-TOP touches a frontal surface of the bubble (Figure 9). Most beams in the S-TOP are discharged in water before the S-TOP touches the bubble frontal surface. Discharged beams are reflected at the air-water interface, and are collected in the S-TOP. When the interface deforms with piercing, the amount of the beam collection decreases; hence, the steep decline of the signal is observed. The peak level of the pre-signal takes maximum when the S-TOP touches a bubble at its pole (flat surface), and decreases with the touch position shift toward an outer edge of the bubble (Figure 10). By using this, we already developed a method to detect where the S-TOP has touched bubble in a bubbly flow (Mizushima and Saito 2012). In this method, the allowable bubble sizes are from 0.8 to 5 mm in volume-equivalent diameter. This is due to the magnitude of the bubble oscillation, and the penetration limit of the S-TOP into a bubble. Depending on the magnitude of the liquid turbulence, the upper limit becomes smaller.
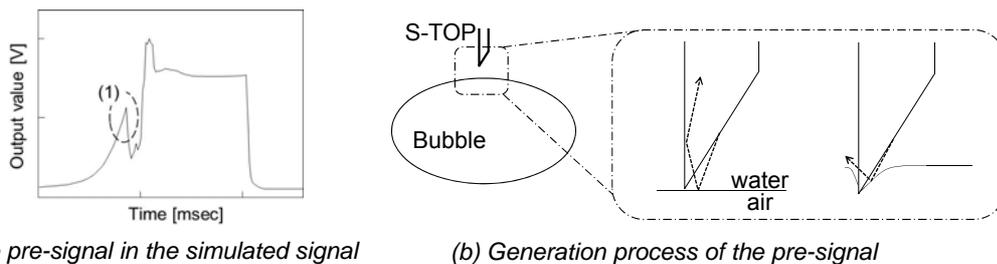

(a) The pre-signal in the simulated signal

(b) Generation process of the pre-signal

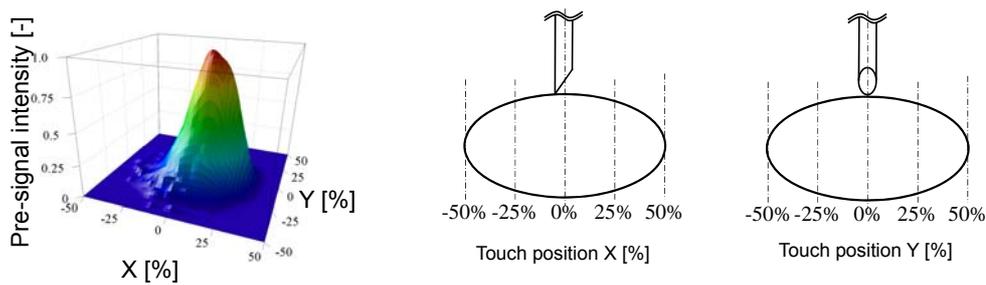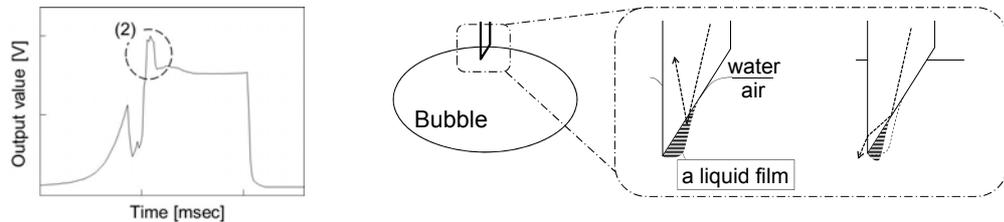Figure 9. Schematic of the pre-signal generation. The amount of re-entering decreases with piercing.

Figure 10. 3D simulated result of relationship between the pre-signal intensity and touch positions.

(2) Spike peak

A spike peak is detected while the S-TOP pierces a frontal surface of the bubble (marked as (2) in Figure 11 (a)). During the piercing, a thin liquid-film forms on the surface of the S-TOP tip. The beams are scattered in the thin film, and re-enter into the S-TOP. The peak level of the spike peak deeply relates to the dynamics of the liquid-film on the tip surface. The spike peaks are detected more often than the pre-signal in a practical use of OFP. In most researches, the peaks are regarded as outliers (despite common signals in OFP). The spike peak is mainly caused by the wettability of the fibre feature; hence, to remove this kind of spike peak, a water repellent treatment for OFP is recommended.

(a) The spike peak in the simulated signal   *(b) Generation process of the spike peak*

Figure 11. Schematic of the spike peak generation. The liquid film forms and moves with piercing. Corresponding to the film behaviour, the spike peak appears and disappears.

6. Conclusion

We analysed the S-TOP signal via 3D ray tracing simulation, in order to improve practical performance of the S-TOP measurement. We investigated the wave patterns carefully and found that noise-like signals arise from optical phenomena between the S-TOP and air-water interface. Mechanisms of the pre-signal and spike peak were clarified. As a result, we were able to educe buried information which is unthinkable or impossible in the existent OFP method; i.e. detection of the touch position. To improve the OFP measurement, it is necessary to consider why the noisy peak occurs, and how it is worth to use or avoidable. Revealing hidden potential of the OFP must bring more promising measurement method for gas-liquid two phase flows. We will provide more advanced OFP measurement numerically and experimentally.

References

Ruoppolo G., Cante A., Chirone R., Miccio F., Stanzione V., 2011, Fluidized Bed Gasification of Coal/biomass Slurries, Chem. Eng. Trans., 24, 13–18.

Nikazar, M., Davarpanah, L., Vahabzadeh, F., 2008, Biosorption of Aqueous Chromium (VI) by Living Mycelium of Phanerochaete Chrysosporium, Chem. Eng. Trans., 14, 475–480.

Mizushima, Y., Saito, T., 2012, Detection method of a position pierced by a single-tip optical fibre probe in bubble measurement, Meas. Sci. Technol., 23, 085308.

Sakamoto, A., Saito, T., 2012, Analysis of optical fiber probing based on a ray tracing, Rev. Sci. Instrum., 83, 075107.

Vejražka, J., Večeř, M., Orvalho, S., Sechet, P., Ruzicka, M.C., Cartellier A., 2010, Measurement accuracy of a mono-fibre optical probe in a bubbly flow, Int. J. Multiphase Flow, 36, 533-548.